International Journal of Heat and Mass Transfer 133 (2019) 36–51

Contents lists available at ScienceDirect

International Journal of Heat and Mass Transfer

journal homepage: www.elsevier.com/locate/ijhmt

Subcooled flow boiling in horizontal and vertical macro-channel under Earth-gravity and hyper-gravity conditions

Maria C. Vlachou [a], John S. Lioumbas [a], Margaritis Kostoglou [a], Kostantinos David [b], Dimitrios Chasapis [b], Christian Schwarz [c], Jack J.W.A. van Loon [c,d], Thodoris D. Karapantsios [a,*]

[a] Division of Chemical Technology, Faculty of Chemistry, Aristotle University of Thessaloniki, University Box 116, 54124 Thessaloniki, Greece
[b] Mechanical Engineering Department, Technical University of Serres, 62124 Serres, Greece
[c] European Space Agency Technology Center (ESA-ESTEC), TEC-MMG LIS Lab, Noordwijk, the Netherlands
[d] DESC (Dutch Experiment Support Center), Department of Oral and Maxillofacial Surgery/Oral Pathology, VU University Medical Center & Academic Centre for Dentistry Amsterdam (ACTA), Amsterdam Movement Sciences, Amsterdam, the Netherlands

ARTICLE INFO

Article history:
Received 19 January 2018
Received in revised form 6 December 2018
Accepted 12 December 2018
Available online 19 December 2018

Keywords:
Flow boiling
Boiling incipience
Inclination
Heat transfer coefficient
Acceleration
(Hyper-)gravity
Buoyancy

ABSTRACT

This is an experimental study on highly subcooled flow boiling of water for assessing the effect of gravitational acceleration on flow boiling heat transfer. The experiments are conducted in a macro-channel 3 mm high, 40 mm wide and 120 mm long at water mass fluxes of 330, 630 and 830 kg/m^2 s and heat fluxes in the range 200–900 kW/m^2. Increased gravitational accelerations, from 1.8 to 9 times the Earth-gravity are achieved with the use of a ~3 m radius centrifuge (Large Diameter Centrifuge, ESTEC/European Space Agency). Two distinct channel inclinations are examined; horizontal, where the gravitational acceleration is normal to the boiling surface, and vertical, where the gravitational acceleration is parallel to the boiling surface and opposite to flow direction. Experiments at hyper-gravity conditions show that for the horizontal channel inclination, flow boiling heat transfer coefficient increases, whereas for the vertical channel inclination it decreases. The observed deviations lie approximately between +15% and −40% from the Earth-g value. An interpretation of the present results is attempted based on the effect of liquid-phase natural and forced convection combined with the effect of buoyancy at vapor bubbles. The tendency of the heat transfer coefficient experimental data with respect to changes in gravitational acceleration allows the development of a gravity-modified version of the well-known two phase model of Liu-Winterton, by incorporating a linearly dependent gravity multiplier.

1. Introduction

Over the last decades, flow boiling has become the most popular heat transfer method in small scale (mini- and micro-channels) [1–5] and in large scale (conventional/macro-channels) cooling applications [6–9]. The reason is that flow boiling combines the benefit of phase change heat transfer – removal of high heat loads through refrigerant's latent heat of vaporization – with the benefit of forced convective heat transfer – transfer of sensible heat in the flowing refrigerant. Buoyancy is among the parameters that dictate flow boiling heat transfer, because it affects [10]:

- Vapor bubbles growth/coalescence/sliding over the boiling surface and detachment.
- Relative motion between vapor bubbles and surrounding liquid (i.e. agitation in the thermal boundary layer over the boiling surface).
- Natural convection of hot liquid layers.

Flow boiling devices that are designed to work at 1-g (Earth-gravity) operate differently at other gravity conditions, e.g., in space (micro-gravity) or during the launch of rockets and accelerating vehicles (hyper-gravity). For the improvement of the performance of flow boiling systems under varying gravity conditions, a systematic investigation of the effect of gravity on flow boiling heat transfer is necessary. So far, several works have examined flow boiling of various refrigerants, yet none of water, under the hyper-gravity periods provided during parabolic flights [11–16]. However, in parabolic flights each parabola offers exposure time slots of less than 20 s to a narrow range of hyper-gravity levels (~1.6–1.8 g). This can create serious transients in boiling investigations. The above disadvantage can be overcome by the use of

* Corresponding author.
E-mail address: karapant@chem.auth.gr (T.D. Karapantsios).

https://doi.org/10.1016/j.ijheatmasstransfer.2018.12.086
0017-9310/

Nomenclature

A	heat exchange area, m^2
A_p	parameter defined by Eq. (16)
ae	gravitational acceleration (g)
Bo	Boiling number ($q'' G^{-1} \Delta H^{-1}$)
C	parameter defined by Eq. (18)
C_p	specific heat, J $kg^{-1} K^{-1}$
D_h	hydraulic diameter, m
f	Darcy friction factor, –
g	gravitational constant, m s^{-2}
G	mass flux, kg $m^{-2} s^{-1}$
Gr	Grashof number ($D_h^3 \rho^2 \beta$ *ae* $(T_{wall} - T_{ave}) \mu^{-2}$)
h	heat transfer coefficient, W $m^{-2} K^{-1}$
k	thermal conductivity, W $m^{-1} K^{-1}$
L	channel length, m
l_e	entrance length, m
LDC	Large Diameter Centrifuge
M	molecular weight, kg mol^{-1}
m	parameter defined by Eq. (24)
N/A	bubble density, m^{-2}
P	pressure, bar
p_r	reduced pressure, – (absolute pressure/critical pressure)
Pr	Prandtl number ($C_p \mu k^{-1}$), –
Q	volumetric flow rate, $m^3 s^{-1}$
q^*	parameter defined by Eq. (17)
q''	heat flux, W m^{-2}
R_{arm}	Gondola's radius of LDC (m)
Re	Reynolds number (ρ u $D_h \mu^{-1}$), –
Ri	Richardson number (*Gr* Re^{-2})
S	parameter defined by Eq. (19)
T	temperature, °C
v	velocity (m/s)
x	channel height, m
w	channel width, m
x	channel height, m

Greek symbols

α	gondola's tilting angle (°)
α_{centr}	centripetal acceleration (m/s^2)
$\alpha_{Coriolis}$	coriolis acceleration (m/s^2)
β	thermal expansion coefficient ($°C^{-1}$)
ΔH	latent heat of vaporization, J kg^{-1}
ΔT	temperature difference, °C
Δx	distance, m
μ	dynamic viscosity, N s m^{-2}
ρ	density, kg m^{-3}
σ	surface tension, N m^{-1}
ω	angular velocity (rad/s)

Subscripts

ave	average
exp	experimental
f	film
FC	forced convection
in	inlet
l	liquid
L-W	Liu-Winterton
mid	middle
mix	mixing cup
OBR	Onset of Bubbly Regime
ONB	Onset of Nucleate Boiling
out	outlet
sat	saturation
sub	subcooling
v	vapor
theor	theoretical
wall	heated wall

centrifugal acceleration equipment (i.e. rotating platforms/trays) to achieve hyper-gravity conditions for much longer time (as long as necessary) and at higher levels than 1.8 g.

To our knowledge, there are two research teams that have reported flow boiling heat transfer results at hyper-gravity conditions accomplished by centrifugal acceleration equipment. Xie et al. [17] conducted two phase heat transfer experiments with *n*-pentane in a transparent helical coil of 8.9 mm diameter under hyper-gravity conditions up to 9 g using a centrifugal plate of 2 m radius. Mass flux ranged between 40 and 200 kg/m^2 s and heat flux was up to 151 kW/m^2. Two configurations of the helical coil were examined; axial, where the helical coil was placed parallel to the direction of rotational acceleration (acceleration through the center of the circles of the coil) and radial, where the coil was placed perpendicular to the direction of rotational acceleration (acceleration parallel to the circles of the coil). These authors showed results depending on the orientation of the experimental set-up; for the radial configuration hyper-gravity enhanced heat transfer with the heat transfer coefficient increasing about from 10 to 60% with increasing acceleration, particularly at low mass flux and low vapor qualities. On the contrary, for the axial configuration an adverse effect was observed and heat transfer coefficients at hyper-gravity were about 40–80% lower than at 1 g. This was attributed to the different relative direction of the centripetal acceleration with respect to the circles of the coils.

Xu et al. [18] and Fang et al. [19] examined flow boiling of R134a up to 3.16 g using the same experimental set-up with a horizontal copper tube fixed onto a centrifugal plate of 1 m radius. The differences between their investigations were (a) on the size of the tube – Xu et al. [18] had a 2.168 mm diameter whereas Fang et al. [19] a 4.04 mm diameter – and (b) on the range of mass fluxes – Xu et al. [18] worked at high mass fluxes (725 and 910 kg/m^2 s) whereas Fang et al. [19] used low mass fluxes (185 and 295 kg/m^2 s). Both works found the heat transfer coefficient to increase with increasing gravitational acceleration between approximately 10 and 40% for gravity levels between 1.12 g and 3.16 g. In addition, Fang et al. [19] noticed that the temperature difference between wall and fluid decreased with increasing gravitational acceleration for the same mass and heat fluxes due to the increasing hydrostatic pressure in their liquid. In addition, they observed a wall superheat drop of the order of one degree Celsius. This is in agreement with the known models of Jens and Lottes [20] and Thorn et al. [21] for heat fluxes below 1000 kW/m^2 and for pressures below 3 bars, and is ascribed to a lower wall superheat required for bubble nucleation as liquid pressure increases [22].

Because of the only few experimental studies on the topic, the effect of gravity level on flow boiling heat transfer mechanism is not yet well understood. Contradicting observations have been made for different working parameters such as channel orientation, liquid pressure and mass flux [17–19]. In addition, water has never been examined as working fluid in flow boiling experiments under hyper-gravity conditions; although it appears to be essential for space and other applications that require instant cooling of high heat loads at high temperatures (i.e. fire incidents).

The scope of the present work is to examine the influence of hyper-gravity conditions (up to 9 g), on subcooled flow boiling heat transfer characteristics (onset of nucleate boiling, boiling curve, and heat transfer coefficient) in a macro channel at horizontal and vertical inclination with water as working fluid. Hyper-gravity is generated by a Large Diameter Centrifuge (LDC, ESTEC/European Space Agency) and experiments are performed under various mass and heat fluxes. The investigated wide range of parameters permits identification of working conditions that enhance heat transfer performance and increase the efficiency of flow boiling devices. In addition, experimental results of heat transfer coefficient under hyper-gravity conditions are compared with predictions of well-known Earth-gravity models.

2. Experimental description

2.1. Large Diameter Centrifuge

Hyper-gravity environment is achieved by the Large Diameter Centrifuge (Fig. 1a), which is located at ESTEC/ESA premises (Noordwijk, NL). The test part of the experimental device is housed in one of the available freely swinging gondolas (A), which tilts more at angle, α, the higher the rotation speed of the centrifuge, in order to cancel the tangential acceleration component and leave only the normal acceleration component acting on the spinning items, Fig. 1b. The centrifuge's arm radius, R_{arm}, is 2.92 m. In addition, the LDC accommodates a central non-tilting gondola (Fig. 1a-B) and two utility cages (Fig. 1a-C) at the sides of the central gondola where auxiliary equipment is placed that cannot sustain high-g levels, e.g., standard computers. The present experiments take place at preselected gravitational accelerations, *ae*, of 1.8, 3, 6 and 9 g.

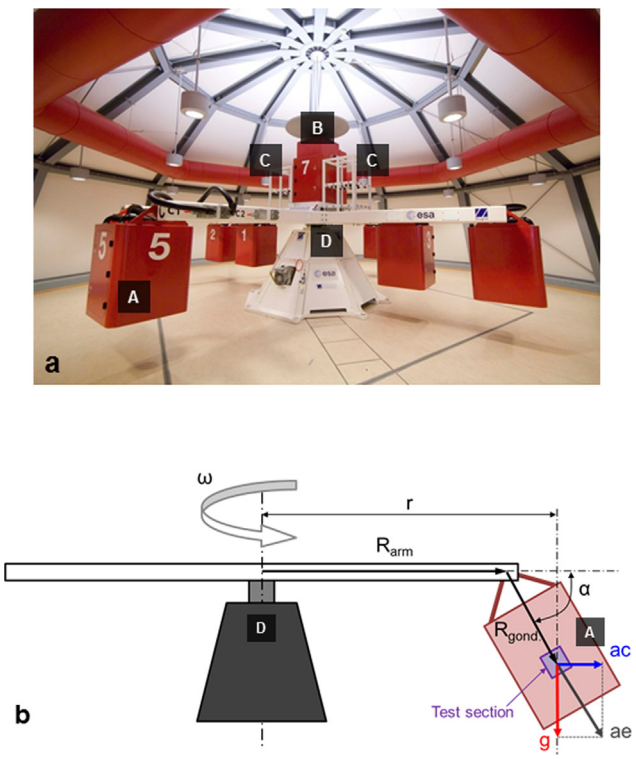

Fig. 1. (a) Photograph of the Large Diameter Centrifuge and (b) schematic graph of the gondola tilt when under rotation. *(A) gondola, (B) central no tilting gondola, (C) utility cages and (D) main structure.*

2.2. Experimental device

The experimental device is illustrated in Fig. 2. It consists of the test section, which is placed inside the gondola and the flow loop, which connects the test section with parts that are placed in the central gondola and the utility cages. A total amount of 120 L of deionized water is stored in the supply tanks (60 L) placed in utility cages on either sides of the central gondola. Degassing of water does not take place, because it is not easy to degas such large volume of liquid (120 L) and then keep it gas free until the end of the experiment. Water is circulated by a centrifugal pump, located beneath the cage, through flexible ½ inch polypropylene tubes, along the centrifuge's arm. Water enters the gondola from a special port, and is guided to the boiling test section. Flow rate is controlled by an inverter (GD10 invt). The water at the outlet of the test section is led out of the gondola through similar flexible tubes, exits through the same special port, and ends up to the return tanks (60 L).

The test section (Fig. 3) is composed of the boiling channel (e) of orthogonal cross-section (x3 mm, w40 mm, L120 mm) and the unheated entrance section (c) of the same cross-section offering sufficient length to achieve fully developed flow (l_e = 250 mm), much longer than required based on the $l_e/D_h > 10$ criterion [23]. The channel is formed by of a copper block (heater) coupled with an aluminum frame of Π shape that is tightly fixed over the copper block. The top, plane surface of the copper block (40 × 120 mm) acts as the boiling surface yielding one sided heating to the flowing water. The aluminum frame has transparent ceramic windows (Schott Robax®) from all three sides to allow optical observations. Electrical heating is achieved by 14 cartridge heaters accommodated inside the copper block capable of delivering maximum

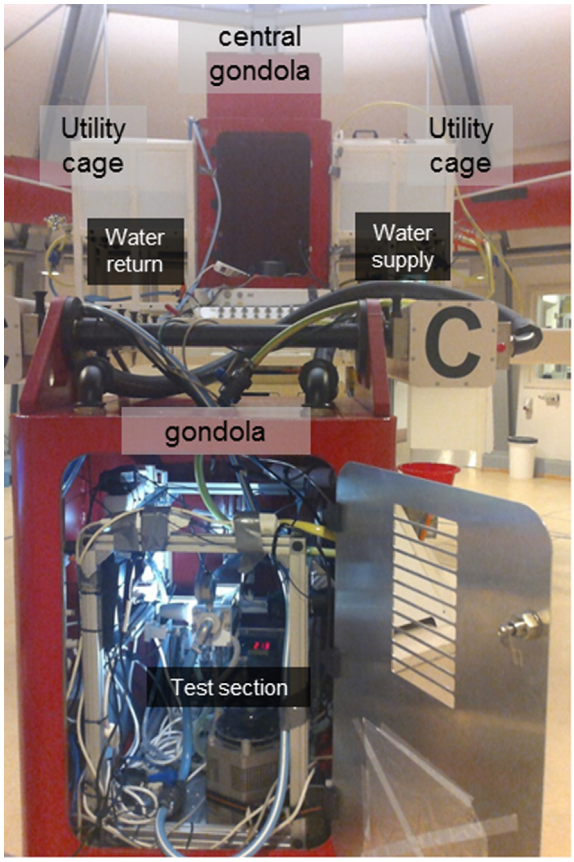

Fig. 2. The experimental device inside a gondola of the Large Diameter Centrifuge.

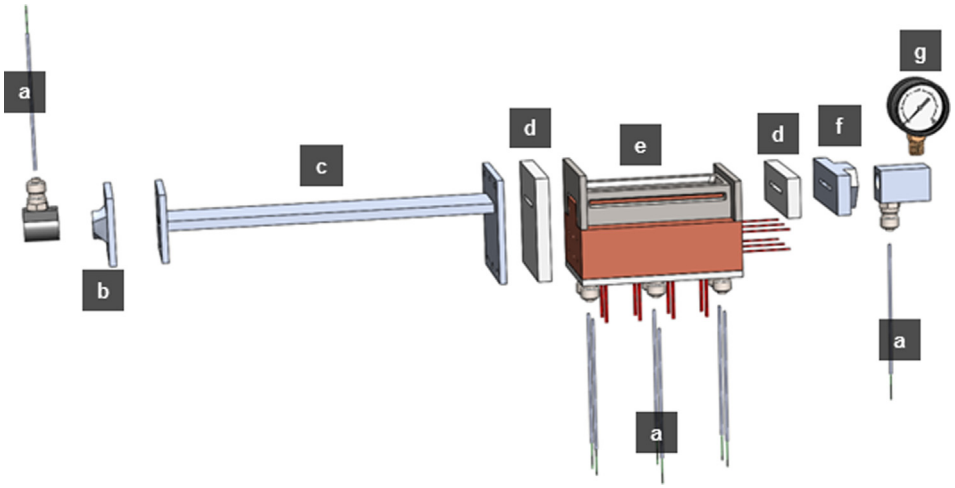

Fig. 3. Schematic graph of the flow boiling test section. *(a) K-type thermocouples, (b) adaptor from circular to orthogonal cross-section, (c) entrance section, (d) Teflon insulation flanges, (e) boiling channel (height:3× width:40× length:120 mm), (f) adaptor from orthogonal to circular cross-section and (g) pressure gauge.*

power of 5.5 kW (heater configuration is provided in Supplementary Fig. S1). Heat flux is controlled by activating different combinations of cartridge heaters and by fine adjustment of the supplied voltage with a variac controller. More details about the test section can be found in Vlachou et al. [8].

Volumetric flow rate is measured by a paddle wheel transmitter (Burkert 8035, range 0.3–10 m/s, accuracy ± 2.5% of measured value). Pressure is monitored by a pressure gauge (Wika, EN 837-1, 0–2.5 bar, accuracy after calibration ± 0.01 bar) at the outlet of the channel. Working fluid and heated wall temperatures are obtained by K-type, ungrounded thermocouples (Uteco, 2 mm, accuracy after calibration ±0.1 °C). The temperature of the working fluid is acquired at the inlet of the entrance section and at the outlet of the channel. The temperature inside the copper block is measured at 6 positions by pairs of thermocouples; 10 mm after the inlet, in the middle, and 10 mm before the outlet of the channel, all placed 2 mm below the boiling surface except from one of the two middle thermocouples, which is placed 12 mm below the boiling surface. A high speed video camera (Mikrotron, Motionblitz, Eosens mini 2, 60 mm macro lens, 8000 fps) and a digital still camera (Basler, ace acA2040-25gm) are employed to record bubbles characteristics from the side window of the channel, 10 mm before the channel's outlet. The still camera views the boiling surface exactly from the side whereas the high speed camera from a small angle shooting the interior of the boiling surface.

2.3. Experimental procedure

Experiments begin by starting the pump and adjusting the flow rate to the desired value and by powering the heaters at a certain value. Then, rotation of the LDC begins, and a waiting period of 10 min is allowed to achieve steady state conditions. Rotation causes an increase in pressure inside the flow loop due to hydrostatic effect. The observed variation of liquid pressure with gravitational acceleration is provided in Supplementary Fig. S2. When steady conditions are reached, continuous recordings of flow rate and temperature are made for a period of 1 min. Still photos in addition to high speed video recordings are obtained for intermittent periods of 1 s. Unfortunately, due to technical and time restrictions of the LDC, it was not possible to obtain good quality optical recordings for all experimental conditions. At every set of experimental conditions at least three runs are conducted to check for repeatability and allow estimation of statistical quantities. Instead of having error bars at each point, error bars are added in the top of the plots representing the average standard deviation of data sets.

Table 1 summarizes the employed experimental conditions. The water flow direction is the same as the acceleration direction (from the center of the LDC arm towards its edge). It is reminded that due to the free swinging of the gondola, at every rotation speed of the LDC the achieved acceleration acts exclusively normal to the boiling surface. Horizontal inclination (0°) is considered the position of the channel which is normal to the direction of the achieved acceleration. Vertical inclination (90°) is considered the position of the channel which is parallel to the achieved acceleration vector. In the latter case, the flow direction is opposite to the direction of acceleration. Although the flow direction is not aligned with the rotating speed, the LDC is designed in such way to minimize Coriolis acceleration generated in the span wise direction of the flow. Nonetheless centripetal and Coriolis forces are given by:

$$a_{centr} = \omega^2 r \tag{1}$$

$$a_{Coriolis} = \frac{2v\omega}{g} \tag{2}$$

where ω is the angular velocity of rotating system (rad/s), r is the radius (m) (arm length plus gondola length due to gondola's free swing), v is the velocity of the moving object (m/s) (attached to the LDC) and g is the acceleration due to gravity (m/s^2) (Fig. 1b). Hyper-gravity environment is achieved by rotational speed ranging from ~19.7 rpm for the lowest, to ~47.9 rpm for the highest

Table 1
Experimental conditions.

Parameter	Value/Range	Unit
Subcooling inlet, ΔT_{sub}	70 (1.0 g), 75 (1.8 g), 79 (3.0 g), 87 (6.0 g), 95 (9.0 g),	°C
Subcooling outlet, ΔT_{sub}	52.2–94.0	°C
Mass fluxes, G	330, 630, 830	kg/m^2 s
Liquid velocity, μl	0.33, 0.63, 0.83	m/s
Reynolds numbers	2500–6500	–
Heat fluxes, q″	200–900	kW/m^2
Channel dimensions	x3, w40, L120	mm
Inclinations	0, 90	°
Gravitational acceleration, *ae*	1, 1.8, 3, 6, 9	g

hyper-gravity condition (Supplementary Table S3) and high arm length, ~3 m. As a result, boiling bubbles are subject to weak Coriolis acceleration, which is estimated to be 0.02–0.04 m/s^2, therefore negligible. In addition, for the vertical inclination case, the test section is subject to a variable hyper-gravity field, due to the different distance from the bottom of the gondola. The deviation of gravitational acceleration at the channel's inlet is estimated from Eq. (3) to be around 30% of the set point (1.8, 3.0, 6.0, 9.0 g) at the channel's outlet (Supplementary Table S3).

$$\Delta(ae) = \frac{\omega^2 \Delta(r)}{\cos(a)} \tag{3}$$

3. Data reduction and empirical models

The quantities directly measured are the volumetric flow rate, Q, outlet pressure, P, temperature inside the heater, T, at several locations, and local temperature of the working fluid at the inlet, T_{in}, and outlet, T_{out}.

Mixing-cup outlet temperature, T_{mix}, is necessary for the estimation of the average bulk temperature of water. T_{mix} represents an average water temperature at the channel's cross-section that depends on mass flux. In a previous work [8] it has been shown that in our experimental setup T_{mix} is linearly correlated with T_{out}, the latter being measured by a thermocouple immersed half-way across the channel width and height at the exit of the heated section. At Vlachou at al. [8], T_{mix} was measured immediately after an in-line static mixer (Koflo, 1 in – 6 elements), which was installed at the exit of the heated section. The relationship between T_{mix} and T_{out} is illustrated in Supplementary Fig. S4. Due to space limitations in the LDC gondola, it was not possible in the present experiments to install an in-line static mixer and so T_{mix} is estimated through its relationship with T_{out}.

Average bulk liquid temperature, T_{ave}, and film temperature between the liquid and the heated wall, T_f, are estimated as follows

$$T_{ave} = \frac{T_{in} + T_{mix}}{2} \tag{4}$$

$$T_f = \frac{T_{wall} + T_{ave}}{2} \tag{5}$$

Temperature differences of subcooling, ΔT_{sub} and wall superheat, ΔT_{wall}, are

$$\Delta T_{sub} = T_{sat} - T_{in} \tag{6}$$

$$\Delta T_{wall} = T_{wall} - T_{sat} \tag{7}$$

ΔT_{sub} is the temperature difference between the working fluid temperature at the inlet and its saturation temperature at the working pressure. ΔT_{sat} is the excess from the boiling point temperature. T_{sat} is the saturation temperature at the liquid's pressure which varies with the hyper-gravity level. T_{wall} is the average wall temperature that occurs from five temperature measurements, after applying Fourier law of conduction for the 2 mm distance between the thermocouples and the heater wall.

The heat flux provided to the liquid, q″, is calculated by Fourier law using as inputs the measured temperature difference of the two middle thermocouples that are positioned 10 mm apart from each other in the direction of heat flow.

$$q'' = -k\frac{\Delta T}{\Delta x} \tag{8}$$

k is copper's thermal conductivity.

The average flow boiling heat transfer coefficient, h, is calculated for the average wall temperature and the average water temperature, representing the combined overall effect of subcooling, forced convection and boiling:

$$h = \frac{q''}{T_{wall} - T_{ave}} \tag{9}$$

The mass flux, G, is

$$G = \frac{Q \cdot \rho_{in}}{x \cdot w} \tag{10}$$

Nusselt number for estimating the forced convective heat transfer coefficient is calculated by linear regression [24] using Schlünder equation (Eq. (11)) for Re = 2300 and either Gnielinski [25] (Eq. (12)) or Dittus-Boetler [26] equation (Eq. (13)) for Re = 10,000. In Eq. (14) the hydraulic diameter is used as the characteristic length of the heated geometry [27]. Forced convective models' tolerances range between ±15 to ±20%:

$$Nu = \sqrt[3]{3.66^3 + 1.61^3 \cdot Re \cdot Pr\frac{D_h}{L}}\left(\frac{Pr}{Pr_{wall}}\right)^{0.11} \tag{11}$$

$$Nu = \frac{\frac{f}{8} Re \cdot Pr}{1 + 12.7\left(\frac{f}{8}\right)^{1/2}\left(Pr^{2/3} - 1\right)}\left[1 + \left(\frac{D_h}{L}\right)^{2/3}\right]\left(\frac{Pr}{Pr_{wall}}\right)^{0.11} \tag{12}$$

$$Nu = 0.023 \cdot Re^{0.8} \cdot Pr^{0.4}\left[1 + \left(\frac{D_h}{L}\right)^{2/3}\right]\left(\frac{Pr}{Pr_{wall}}\right)^{0.11} \tag{13}$$

$$h = \frac{Nu \cdot k}{D_h} \tag{14}$$

where f is the friction factor obtained from Moody's diagram for a smooth pipe, D_h is the hydraulic diameter for orthogonal channel defined as $D_h = \frac{2xw}{x+w}$, L is the heated length, fluid properties are calculated at T_{ave}, Pr_{wall} is calculated at T_{wall} and k in Eq. (14) is calculated at T_f.

Forced convective heat transfer results for single phase liquid flow experiments at 1 g have been used to validate the performance of the experimental device (Fig. 4a and b). MAPE (mean absolute percentage error) from the single phase predictions of Gnielinski equation is 19.4% and of Dittus-Boetler 24.0%. Similar MAPE values are obtained for the hyper-gravity levels of 1.8, 3, 6 and 9 g (Fig. 4c and d) without any clear trend with respect to the hyper-gravity level: for Gnielinski equation MAPE was 19.5, 15.9, 16.1 and 15.6% and for Dittus-Boetler 22.5, 20.9, 21.4 and 16.5%, respectively. It should be noted that although MAPE values are acceptable, estimations for the low mass flux value, 300 kg/m^2 s, appear to be well off the models' tolerance, irrespective the gravitational acceleration level. This is so despite the fact that predictions take into account the short heated length and the high temperature difference between wall and liquid bulk. It must be stressed that entrance effects for transition and turbulent flow are eliminated in these present experiments because l_e/D_h = 50.

Reference values for the heat transfer coefficient in the subcooled flow boiling region are estimated from the empirical correlations of Liu-Winterton [28] (Eqs. (15)–(19)) (model's tolerance ±40%) and Shah [29] (Eqs. (20) and (21)) (model's tolerance ±30%). These equations are developed for 1 g conditions and they do not include any gravity related term. However, in the absence of suitable gravity related expressions, they are examined here if they are valid also for hyper-gravity conditions.

$$h = \frac{\sqrt{(A_P S \Delta T_{wall})^2 q''^{\frac{4}{3}} - q''^2}}{\Delta T_{wall}} \cdot q_*^{\frac{3}{2}} \tag{15}$$

$$A_P = 55 \cdot p_r^{0.12}(-\log p_r)^{-0.55} M^{-0.5} \tag{16}$$

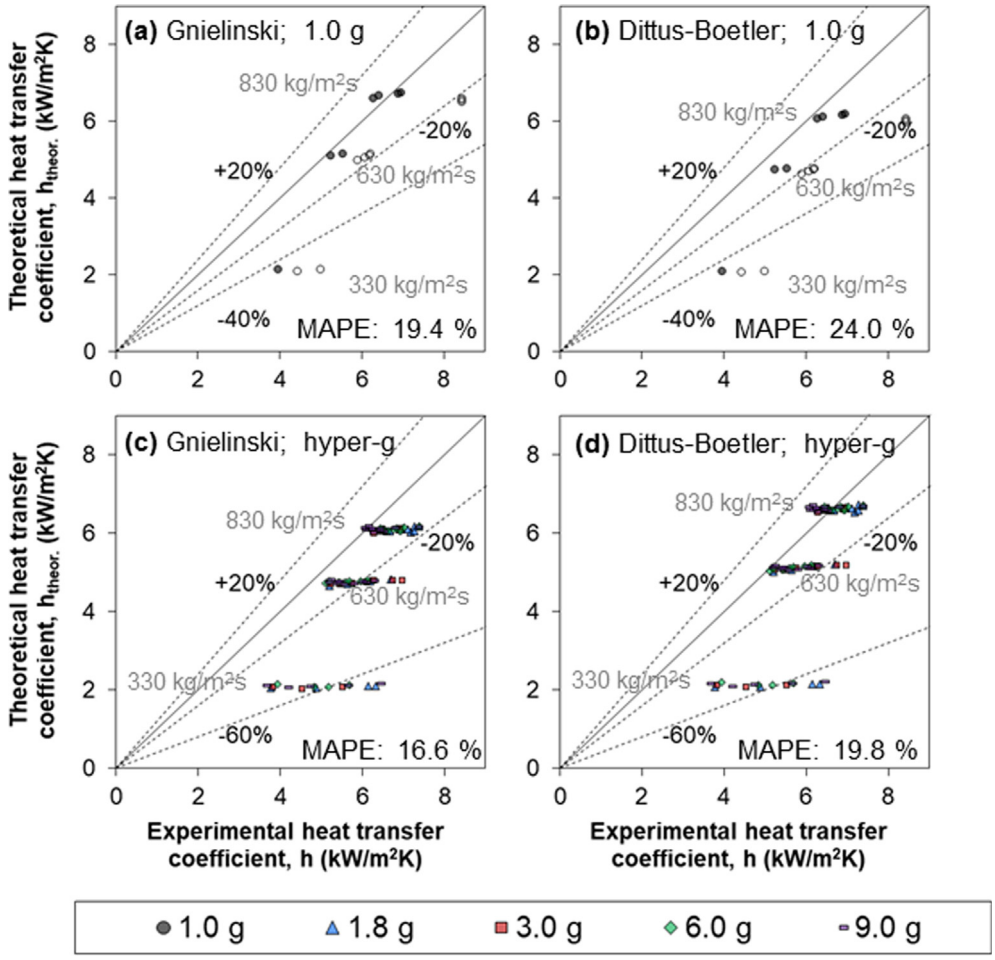

Fig. 4. Comparison between present experimental values of heat transfer coefficient and values estimated from the correlations of (a) and (c) Gnielinski [24], and (b) and (d) Dittus-Boelter [25]. *For figures (a) and (b) empty symbols stand for horizontal and filled symbols for vertical inclination and exclusively for single phase conditions. For figures (c) and (d) data are jointly for the horizontal and vertical inclinations and exclusively for single phase conditions.*

$$q_*^3 - C q_*^2 - 1 = 0 \tag{17}$$

$$C = \left(\frac{A_P S}{h_{FC}}\right)^2 \left[\frac{\sqrt{(A_P S \Delta T_{wall})^2 q^{\frac{4}{3}} - q^2}}{\Delta T_{wall}} \cdot (T_{wall} - T_{aver})\right]^{\frac{4}{3}} \tag{18}$$

$$S = \left(1 + 0.055 Re^{0.16}\right)^{-1} \tag{19}$$

$$h = \frac{h_{FC}(T_{wall} - T_{aver)} + h_{FC}(\psi_0 - 1)\Delta T_{wall}}{T_{wall} - T_{aver}} \tag{20}$$

$$\text{Larger value between } \psi_0 = 230 Bo^{0.5} \text{ and } \psi_0 = 1 + 46 Bo^{0.5} \tag{21}$$

where p_r is the reduced pressure, M the molecular weight, h_{FC} is the forced convective heat transfer coefficient by Dittus-Boetler (Eqs. (13) and (14)) and fluid properties are calculated at T_{ave}.

Mean absolute percentage error, MAPE, between the experimental, h_{exp}, and the predicted value, h_{theor}, of heat transfer coefficient is given by:

$$MAPE = \left[\frac{1}{N}\sum_{1}^{N} ABS\left(\frac{h_{exp} - h_{theor}}{h_{exp}}\right)\right] \cdot 100 \tag{22}$$

4. Results and discussion

4.1. Effect of hyper-gravity on boiling curves

Plotting heat flux, q″, versus wall superheat, ΔT_{wall}, results in boiling curves, which allow comparison of the channel's heat removal capacity at the different experimental conditions. It is reminded that the same ΔT_{wall} does not correspond to the same wall temperature, since the liquid pressure varies with gravity level. Figs. 5 and 6 show the effect of hyper-gravity on the boiling curves for the horizontal and vertical channel inclination, respectively. Additionally, these plots designate also the onset of nucleate boiling, ONB (first bubble's appearance) marked with a blue line, and the onset of bubbly regime, OBR (domination of nucleate boiling), marked with a red line. More details about the determination of ONB and OBR lines and the related heat transfer mechanisms can be found in Vlachou et al. [8]. At both inclinations three values of G have been examined, 330, 630 and 830 kg/m² s, which represent a low, an intermediate and a high mass flux conditions. It is noticeable that the effect of hyper-gravity is different for the two inclinations:

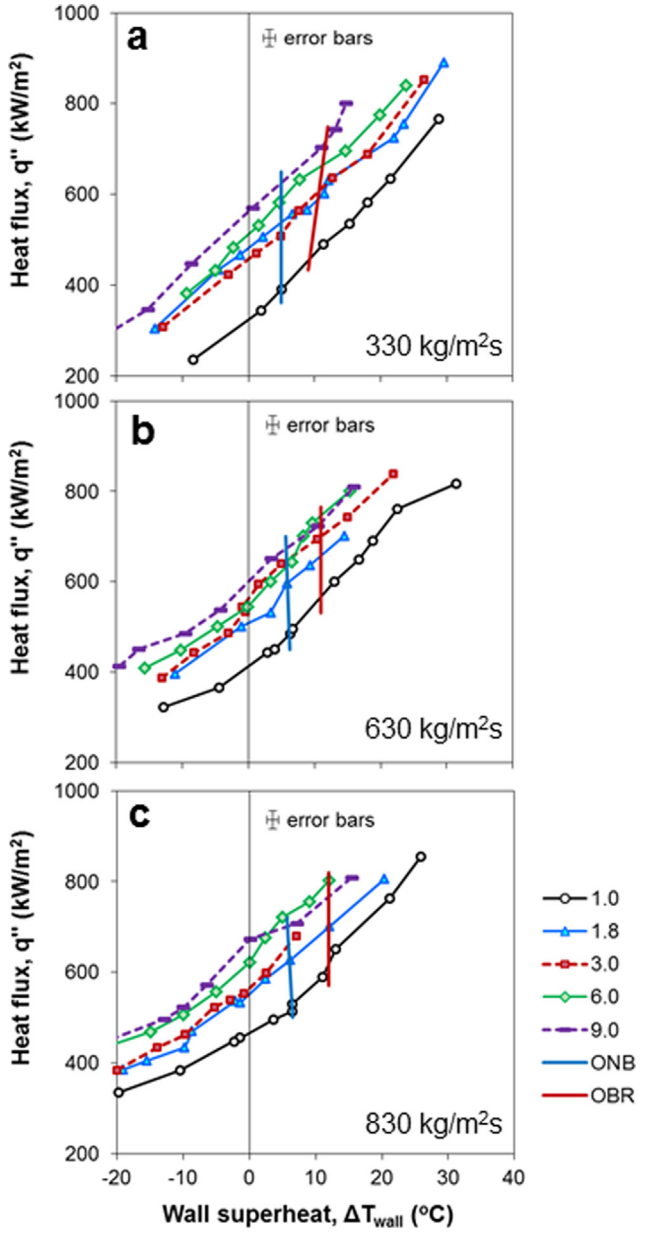

Fig. 5. Effect of gravitational acceleration on boiling curves for horizontal channel inclination and water mass flux at (a) 330 kg/m^2 s, (b) 630 kg/m^2 s and (c) 830 kg/m^2 s. *ONB: onset of nucleate boiling, OBR: onset of bubbly regime. For clarity among lines, only average error bars for all data points are showed at the top of each plot.*

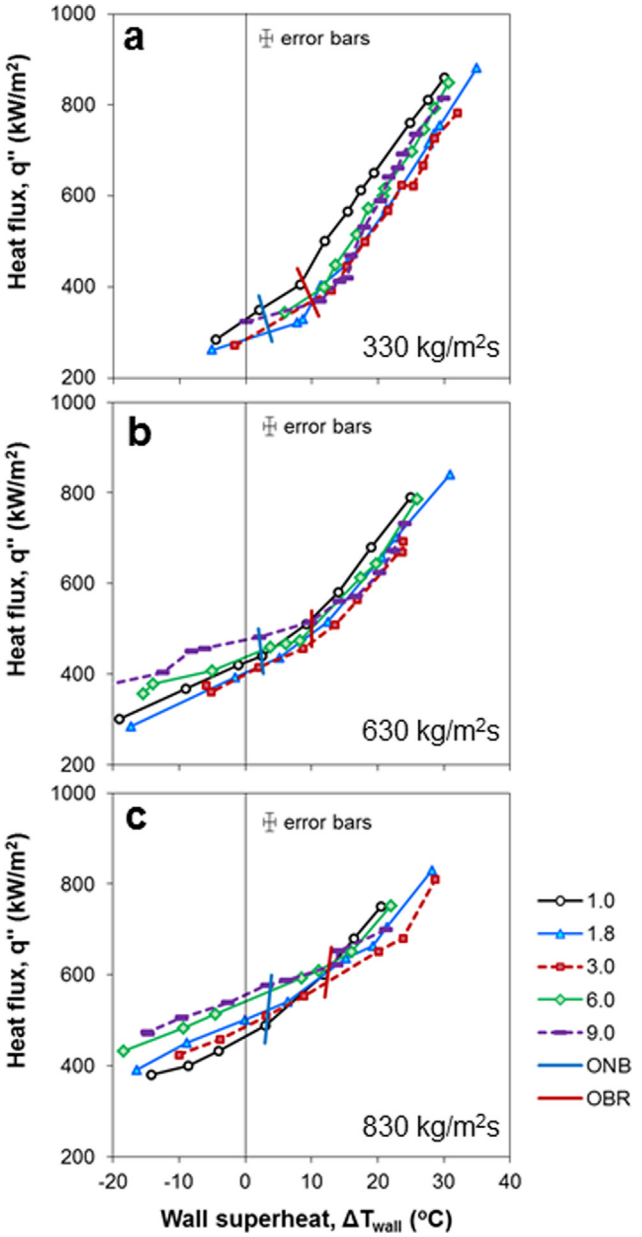

Fig. 6. Effect of gravitational acceleration on boiling curves for vertical channel inclination and water mass flux at (a) 330 kg/m^2 s, (b) 630 kg/m^2 s and (c) 830 kg/m^2 s. *ONB: onset of nucleate boiling, OBR: onset of bubbly regime. For clarity among lines, only average error bars for all data points are showed at the top of each plot.*

- For the horizontal inclination (Fig. 5), when the gravitational acceleration, *ae*, increases the boiling curves shift up and to the left by a small extent, that is, to lower ΔT_{wall}. The effect, however, is not always clear as it sometimes falls within the margin of experimental uncertainty (error bars). Only when *ae* increases from 1 g to 1.8 g the effect is beyond doubt because in this case the horizontal shift of the boiling curve is about 10 °C. The above holds for all three G values.
- For the vertical inclination (Fig. 6), the boiling curves are scattered within a narrow range without a clear dependence on the value of gravitational acceleration, *ae*. Moreover, for quite a few heat fluxes these curves appear to overlap given the margin of experimental uncertainty (error bars). The above holds for all three G values. What is perhaps more interesting is that the 1-g boiling curve appears in most cases to lie above all other curves, indicating a more effective performance at 1 g than at hyper-g (higher heat flux for the same ΔT_{wall}).

ONB and OBR lines in Figs. 5 and 6 represent an average line that goes through the points of ONB and OBR of each boiling curve. These lines in Figs. 5 and 6 seem almost vertical for all cases, meaning that ΔT_{wall} at which ONB and OBR occur is alike, ±~1 °C, among *ae* values (Fig. 7a). This agrees with the findings of Fang et al. [19] but also of Jens and Lottes [20] and Thorn et al. [21] regarding the effect of pressure on ONB for heat flux less than 1000 kW/m^2 and pressure less than 3 bars.

On the contrary, the q″ values at which ONB and OBR occur, vary with *ae*, as shown in Fig. 7b. For the horizontal inclination q″ follows an increasing trend with *ae*, while for the vertical inclination q″ is quite insensitive to *ae*. The trends of q″ with *ae* are sim-

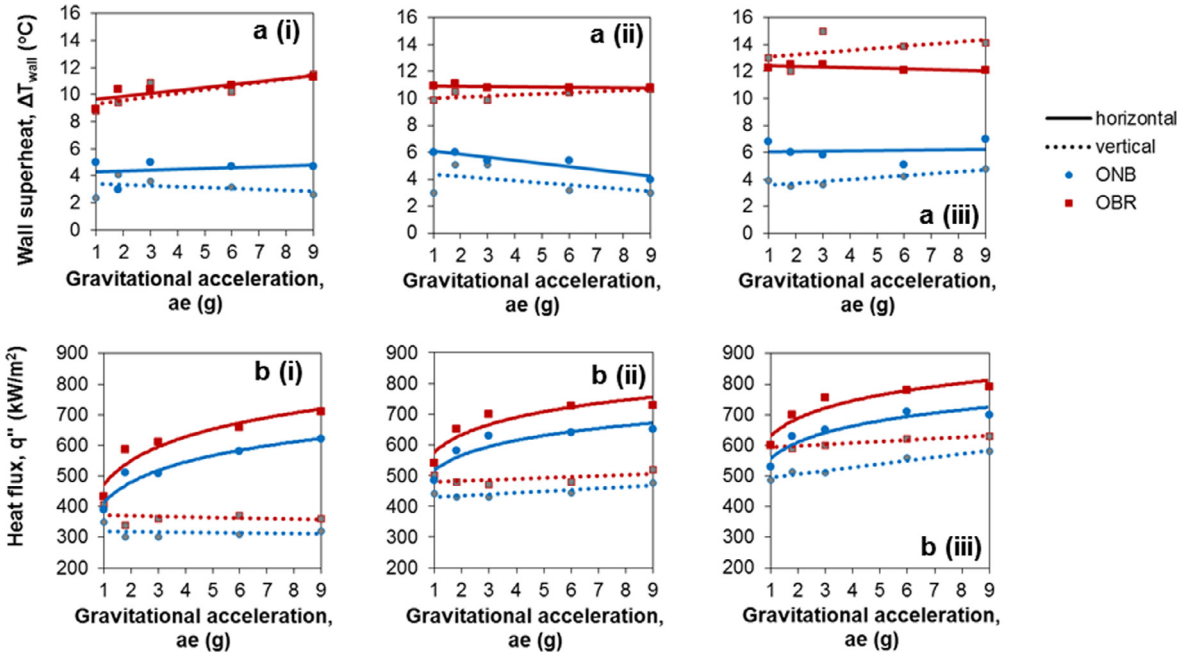

Fig. 7. Effect of gravitational acceleration (a) on wall superheat and (b) on heat flux for the heat transfer regions for horizontal and vertical channel inclinations and water mass flux (i) 330 kg/m^2 s (ii) 630 kg/m^2 s and (iii) 830 kg/m^2 s. *ONB: onset of nucleate boiling, OBR: onset of bubbly regime.*

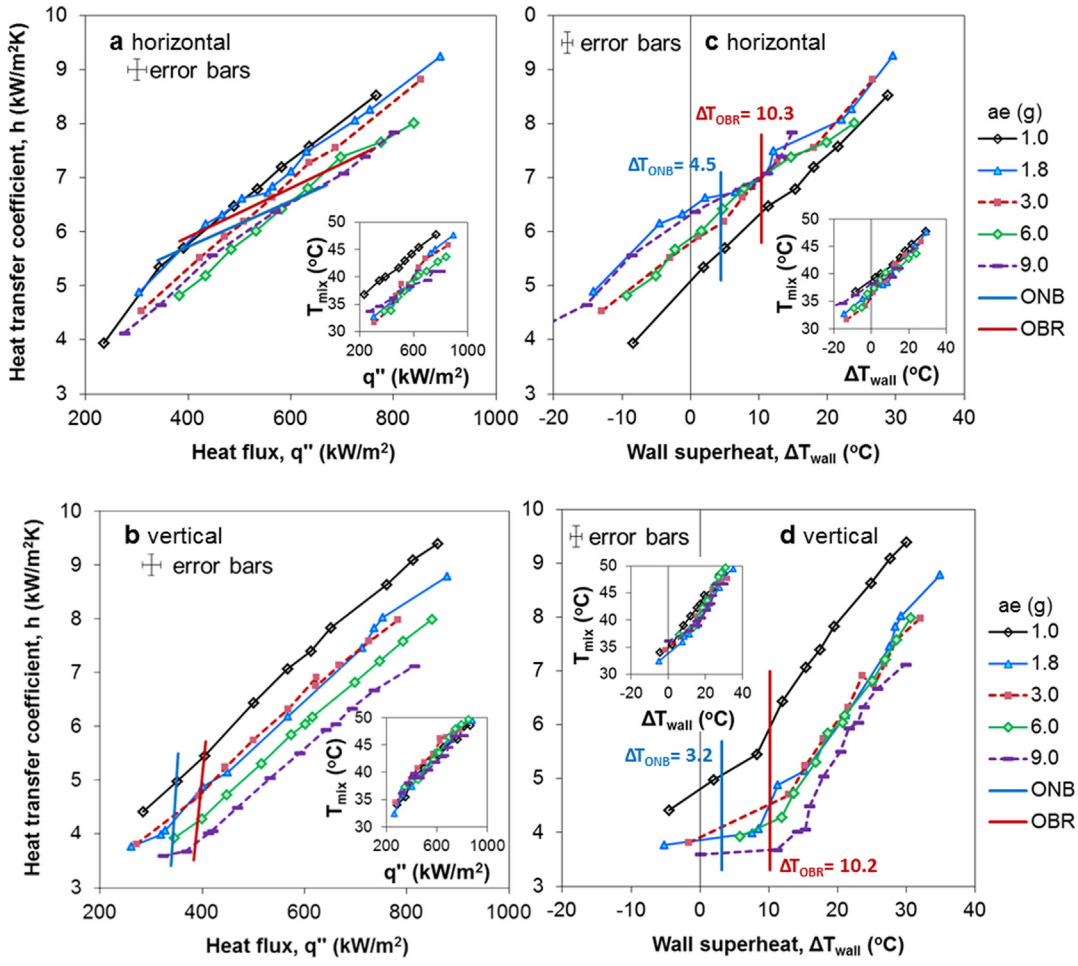

Fig. 8. Effect of gravitational acceleration on heat transfer coefficient for 330 kg/m^2 s water mass flux with respect to heat flux at (a) horizontal and (b) vertical channel inclination and with respect to wall superheat at (c) horizontal and (d) vertical channel inclination. *Inset plots: Effect of gravitational acceleration on water outlet temperature (T_{mix}). ONB: onset of nucleate boiling, OBR: onset of bubbly regime. For clarity among lines, only average error bars for all data points are showed at the top of each plot.*

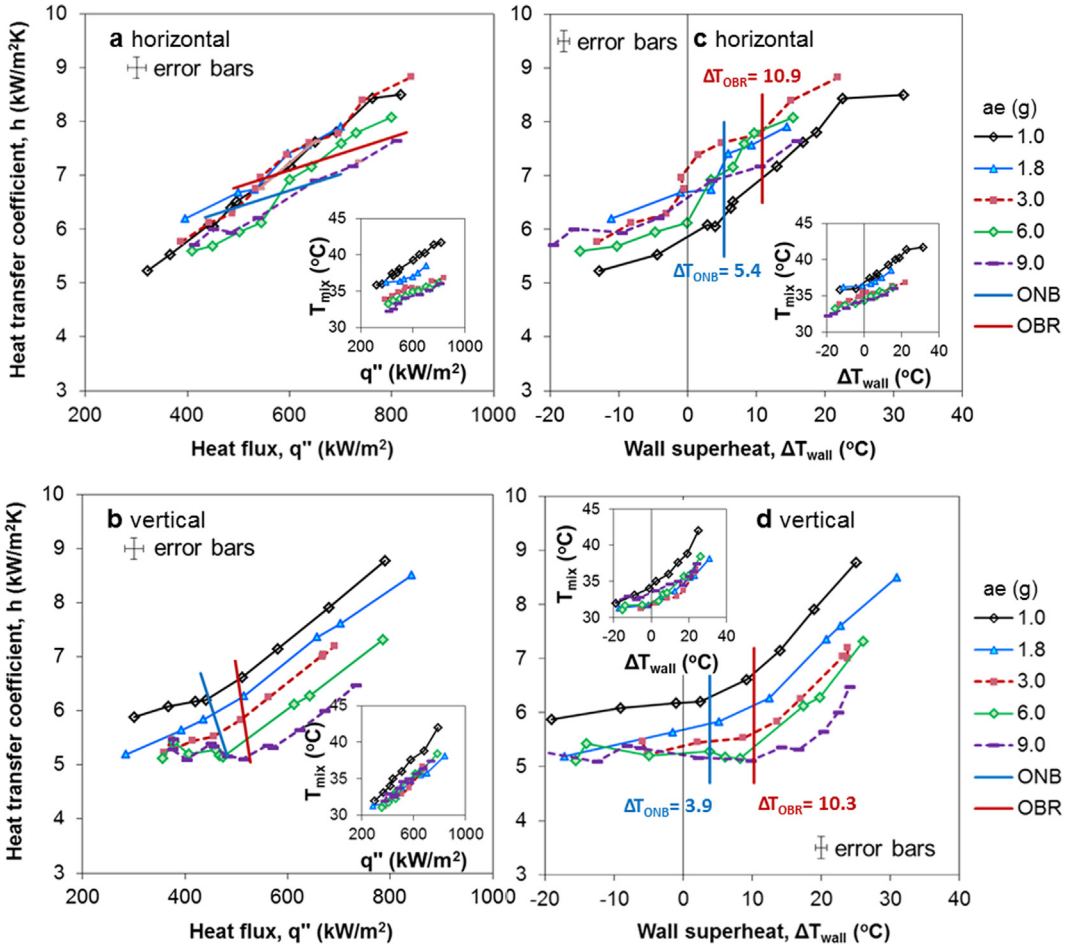

Fig. 9. Effect of gravitational acceleration on heat transfer coefficient for 630 kg/m^2 s water mass flux with respect to heat flux at (a) horizontal and (b) vertical channel inclination and with respect to wall superheat at (c) horizontal and (d) vertical channel inclination. *Inset plots: Effect of gravitational acceleration on water outlet temperature (T_{mix}). ONB: onset of nucleate boiling, OBR: onset of bubbly regime. For clarity among lines, only average error bars for all data points are showed at the top of each plot.*

ilar among G values: In all cases, the difference in q″ between ONB and OBR is small (transition region), showing that shortly after boiling incipience, nucleate boiling becomes the dominant heat transfer mechanism (OBR designates the domination of nucleate boiling, as discussed in previous works [8,9]). At 1 g the heat flux values of the transition region for the horizontal and the vertical channel are close to each other, but as *ae* increases, the transition region for the horizontal channel shifts to higher q″. This indicates that as *ae* increases, boiling emerges and intensifies at much higher q″ for the horizontal than for the vertical inclination. Consequently, as *ae* increases, the Critical Heat Flux increases appreciably for the horizontal inclination, whereas only slightly for the vertical inclination.

At first glance, hyper-gravity affects positively flow boiling heat transfer when the direction of the gravitational acceleration is normal to the heated surface (horizontal channel), but it does not affect, or even affects negatively, flow boiling heat transfer when the direction of the gravitational acceleration is parallel to the heated surface (vertical channel). The enhancement observed at the horizontal inclination may be attributed to three mechanisms (a) buoyancy that hastens bubbles detachment, (b) increased local turbulence created by the fast departure of bubbles [14], and (c) intensified natural convection in the liquid phase which widens the thermal boundary layer over the boiling surface [30]. The latter seems to play a key role since there is heat transfer enhancement also in the absence of bubbles (before ONB) and even for negative wall superheats, Fig. 4. For the vertical channel inclination where the flow has the same orientation with the gravitational acceleration but an opposite direction, the above mechanisms are rather suppressed. This is because in the direction of the flow, forced convection forces are stronger than natural convection and buoyancy forces. As a matter of fact, an attempt to quantify it with respect to Richardson number (=Gr/Re^2) has been made. For all working conditions *Ri* is well below 0.1, which is the critical value above which natural convection becomes significant. Especially for the low mass flux, 330 kg/m^2 s, where natural convection is expected to have higher impact, the low *Re* numbers yield, *Ri* numbers between 0.009 and 0.07 (Supplementary Fig. S5) (empty symbols are for horizontal inclination and filled symbols for vertical inclination). It is observed that *Ri* increases with wall superheat (or heat flux for the same wall superheat), but also increases with gravitational acceleration, as expected, due to the increased *Gr*, which reflects the effect of gravity.

Interestingly, other works [11,12] that conducted flow boiling experiments in vertical channels during parabolic flights, found enhancement of heat transfer at hyper-gravity conditions (1.8 g). This was ascribed to increased buoyancy that decreased bubbles size at detachment. However, during each parabola there is less than 20 s exposure to hyper-gravity (slots before and after the microgravity period) where strong acceleration transients and vibrations are possible [31]. Besides, those works focused chiefly on micro-gravity effects, where inclination does not play any role.

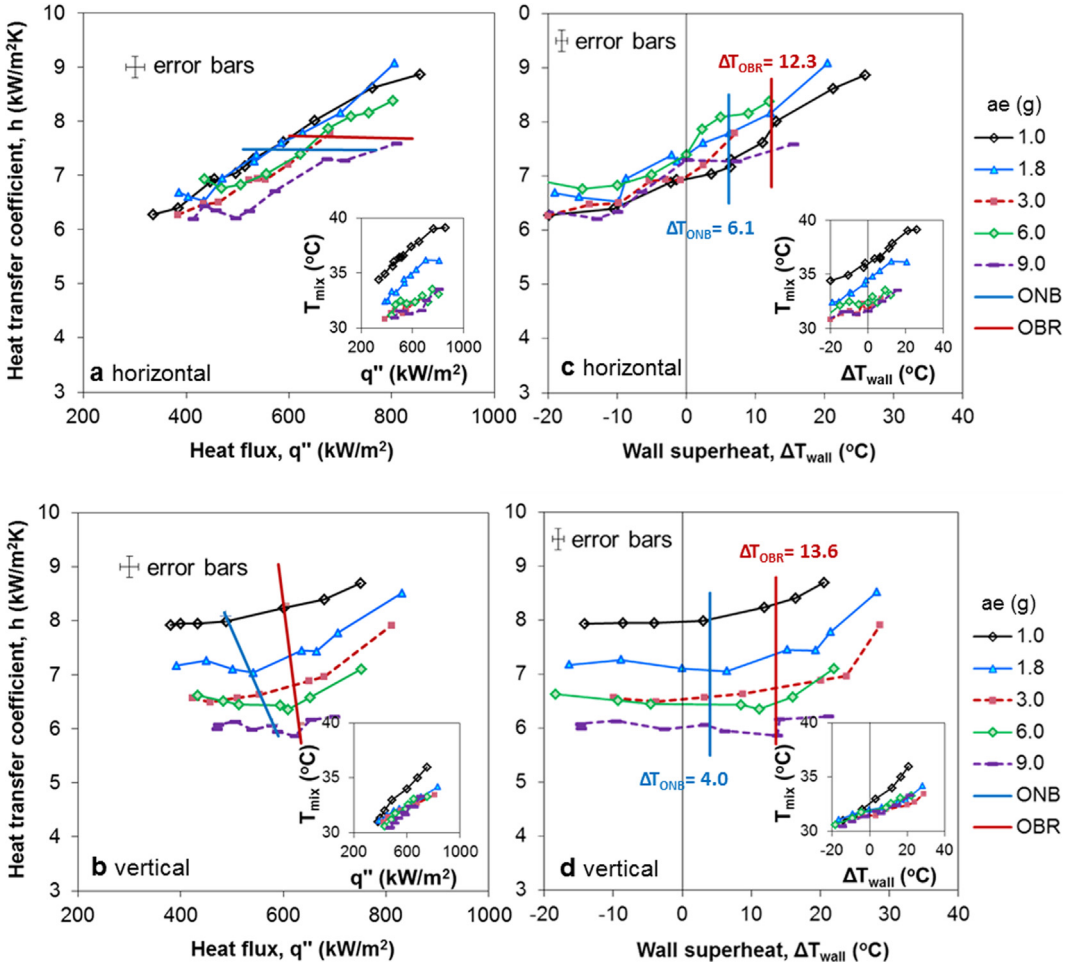

Fig. 10. Effect of gravitational acceleration on heat transfer coefficient for 830 kg/m^2 s water mass flux with respect to heat flux at (a) horizontal and (b) vertical channel inclination and with respect to wall superheat at (c) horizontal and (d) vertical channel inclination. *Inset plots: Effect of gravitational acceleration on water outlet temperature (T_{mix}). ONB: onset of nucleate boiling, OBR: onset of bubbly regime. For clarity among lines, only average error bars for all data points are showed at the top of each plot.*

4.2. Effect of hyper-gravity on heat transfer coefficient

Figs. 8–10 show the variation of h with respect to q″ and ΔT_{wall} for the examined gravitational acceleration, *ae*, and mass flux, G, values. Small inset plots illustrate the respective variation of water's outlet mixing-cup temperature, T_{mix}. Although in literature it is common to present solely h versus q″, here it is decided to present h also versus ΔT_{wall}. This is because in the present experiments as *ae* increases the liquid pressure increases, see S2, and this affects T_{sat}. In other words, as *ae* increases the thermal driving force for heat transfer changes and this can only be seen in the plots of h with respect to ΔT_{wall}.

At the horizontal inclination, for any q″ as *ae* increases h decreases (Figs. 8a; 9a; 10a). This is mostly evident for *ae* > 3 g. However, the picture is different in the behavior of h for any ΔT_{wall} (Figs. 8c; 9c; 10c). In the latter it is seen that when *ae* gets higher than 1 g then h increases but h values are scattered with no clear trend as regards *ae*. For the given experimental uncertainty (error bars), the departure of the 1 g data from the other-g data is less pronounced as mass flux increases from 330 to 830 kg/m^2 s.

At the vertical inclination, the situation changes radically and as *ae* increases then h decreases with respect to both q″ and ΔT_{wall} (Figs. 8b, d; 9b, d; 10b, d). This is more evident in the plots with respect to q″, Figs. 8b; 9b; 10b, whereas in the plots with respect to ΔT_{wall} this trend is benign. For instance, in Fig. 8d, the values of h for *ae* > 1 g are comparable to each other, with only the h values for *ae* = 9 g being systematically lower than the other h values. On the contrary, in Figs. 9d and 10d there is a clear trend for lower h values as *ae* increases, especially at high ΔT_{wall} values.

Fig. 11 shows the percentage variation of h at hyper-gravity compared to h at 1 g with respect to *ae* at horizontal channel inclination. The figure presents data from the current experimental work at four specific ΔT_{wall} values (Fig. 11a-c), which correspond to low (ΔT_{wall} = 5 °C), intermediate (ΔT_{wall} = 10–20 °C) and high q″ (ΔT_{wall} = 25 °C), and data from Xu et al. [18] (Fig. 11d) and Fang et al. [19] (Fig. 11e). It is seen, (Fig. 11a-c), that increasing *ae* from 1 to 1.8 g, increases h abruptly by about 5–15%. The percentage change is, in general, smaller as G increases. The corresponding ΔT_{wall} for ONB and OBR (average values from Fig. 7a) are also displayed in the figures. At ΔT_{wall} = 5 °C for 630 and 830 kg/m^2 s, boiling is not initiated, hence at those conditions there are no bubbles present. Yet, the percentages of increase in h are comparable with the cases where bubbles are present, indicating that the effect of hyper-gravity is prominent not only in the nucleate boiling region (increased buoyancy enhances bubbles detachment causing agitation of the thermal layer close to the heated wall [11,12,30]), but also in the single (liquid) phase flow region (enhanced natural convection [30]). Interestingly, for 1.8 g < *ae* ≤ 9 g, the percentage change of h remains either approximately the same as at 1.8 g or it is reduced compared to that at 1.8 g. In addition, as ΔT_{wall} increases, the percentage variation of h is smaller, which is in line with what was observed by Xu et al. [18] (Fig. 11d) and Fang et al. [19] (Fig. 11e) (lines are for different q″ instead of different ΔT_{wall} but results are equivalent).

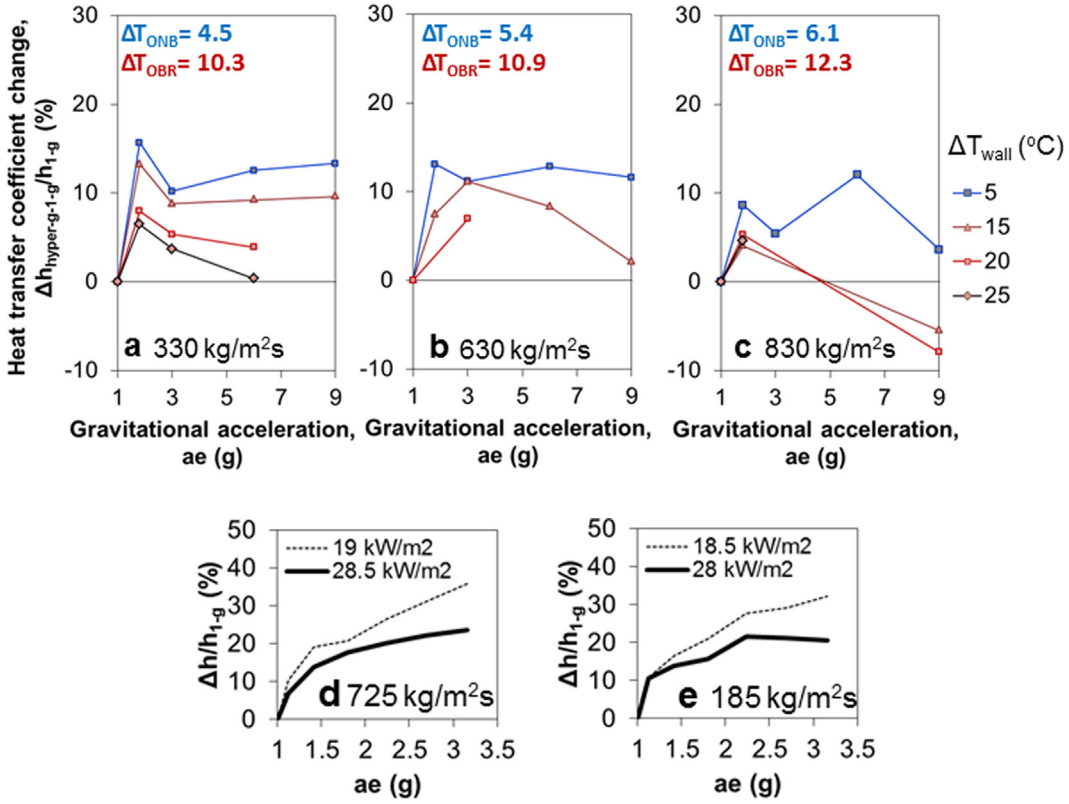

Fig. 11. Percentage change of heat transfer coefficient with gravitational acceleration for horizontal channel inclination and water mass flux at (a) 330, (b) 630, (c) 830 kg/m^2 s (present data), (d) Xu et al. [18] 725 kg/m^2 s and (e) Fang et al. [19] 185 kg/m^2 s. *ONB: onset of nucleate boiling, OBR: onset of bubbly regime.*

Representative photo images of flow boiling regimes under hyper-gravity conditions at horizontal channel inclination are illustrated in Table 2 for 330 kg/m^2 s and Table 3 for 830 kg/m^2 s. It is reminded that due to technical restrictions not all images are available for all experimental conditions. In Table 2, it can be approximately noted that as *ae* increases, bubbles become smaller and their number rises. These changes are not linear with *ae*. Meanwhile, for the same q″ as *ae* increases a decrease in ΔT_{wall} is observed. This drop in ΔT_{wall} is beyond the drop expected for the increased liquid pressure as *ae* increases [20–22] and as already observed for ONB (Fig. 7a). One is tempted to argue that at high *ae* values the intense bubble buoyancy and liquid natural convection facilitate heat removal from the boiling surface at a smaller driving force, i.e., ΔT_{wall}. Supplementary Video S6 shows a high speed video recorded at *ae* = 3 g, G = 330 kg/m^2 s, q″ = 690 kW/m^2 and for horizontal channel inclination. Shooting is made from a small angle above the level of the boiling surface and targets the interior of the boiling surface. Images are highly distorted due to the steep refractive index gradient between the hot boiling surface and the highly subcooled core flow. Nevertheless, it is still possible to observe scattered bubbles nucleating and growing while at the same time they slide along the boiling surface. When bubbles reach a critical size they detach and violently re-condense in the core flow.

At this point it should be mentioned that although a small variation of the degree of subcooling with pressure (acceleration level) does not have an impact on the boiling curves, it might affect bubbles sizes. Yet, previous studies with the present experimental setup [9] at 1.0 g have revealed that due to the high subcooling conditions such small variations in the degree of subcooling have negligible effect on bubble size. Regarding the effect of heat flux on bubble size, it is observed that bubbles size increases up to a roughly maximum size at a certain heat flux above which they do not grow any further. Even in case of coalescence, the size of the produced larger bubbles retrieves to this maximum value because of re-condensation of the excess vapor in the cold bulk liquid. The fact that bubbles size does not increase steadily with heat flux, ceteris paribus, is because bubble density also increases with q″, but this is difficult to see in the 2D side views presented in these tables. Careful inspection of side videos allows a little better perspective of bubble density.

Fig. 12 shows the percentage variation of h at hyper-gravity compared to h at 1 g with respect to *ae*, at vertical channel inclination. Data are for three specific ΔT_{wall} values corresponding again to low, intermediate and high q″ (Fig. 12a-c), as the horizontal inclination. Unfortunately, it was not possible to locate any pertinent literature data for the vertical inclination to compare our data with. For the vertical inclination (Fig. 12a-c), increasing *ae* from 1 g to 1.8 g, causes a decrease in h between roughly 5% and 25%. The only exception is for G = 830 kg/m^2 s and ΔT_{wall} = 5 °C, where a small increase of h is observed. Further increase in *ae* decreases h even more for all cases, but not linearly with *ae*. The percentage variation is larger for lower G, where bubble buoyancy and liquid natural convection (both dictated by the g value) compete more effectively with forced convection (at 9 g $h_{hyper\text{-}g}$ drops at −40% of h_{1-g}). ΔT_{wall} for ONB and OBR (average values from Fig. 7a) are also displayed in the figures. All data in the plots correspond to boiling conditions (bubbles are present), as there is no curve for ΔT_{wall} below ONB. In the vertical channel inclination although buoyancy and natural convection are enhanced by increased gravitational accelerations they are largely masked by the forced convective flow and so do not contribute significantly to heat transfer. A possible explanation for the above is that at the vertical inclination, buoyancy acts in parallel to the boiling surface, enhancing bubbles sliding and coalescence over the boiling surface with hardly any effect on bubbles detachment. The present find-

Table 2
Images for horizontal channel inclination at 330 kg/m^2 s.

ae (g)	q'' (kW/m^2)	ΔT_{wall} (°C)	Photograph from the side window
1.8	600	8.8	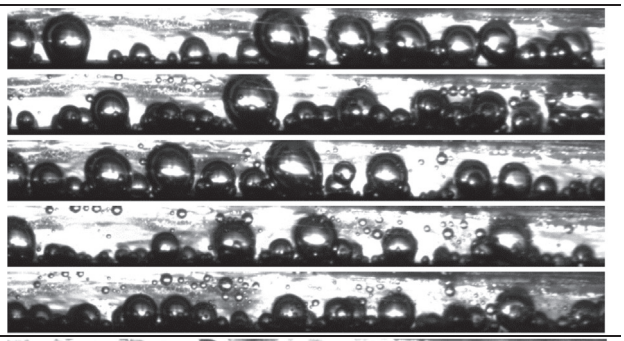
	680	10.2	
	770	22.0	
	850	23.5	
	900	29.6	
3.0	600	6.6	
***	690	12.6	
	770	18.0	
	900	26.6	
6.0	770	14.6	
	940	23.9	
9.0	850	11.1	
	900	14.6	

*** *snapshot of high-speed video recording/ Supplementary S5* 1 mm

Video shoots from a small angle above the boiling surface and targets the interior of the boiling surface

Table 3
Images for horizontal channel inclination at 830 kg/m^2 s.

ae (g)	q'' (kW/m^2)	ΔT_{wall} (°C)	Photograph from the side window
1.8	730	6.0	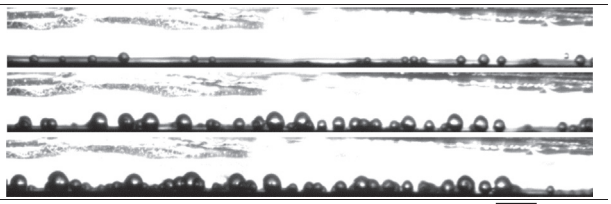
	770	11.6	
	900	16.0	

1 mm

ings disagree with the results from vertical channels obtained in parabolic flights which argue about either heat transfer enhancement [32] or no effect [33] at ~1.6–1.8 g. However, as already mentioned parabolic flights exhibit intense transients and vibrations in their short hyper-gravity periods.

Representative photo images for the vertical channel inclination and mass fluxes 330 and 830 kg/m^2 s are shown in Tables 4 and 5. In Table 5 as *ae* increases bubbles become smaller and greater in number, as was also observed at the horizontal inclination. Through these tables it is possible to compare the performance of the horizontal and vertical inclinations for *ae* = 9 g, G = 330 kg/m^2 s and q″= 900 kW/m^2, as well as for *ae* = 1.8 g, G = 830 kg/m^2 s and q″: 770, 900 kW/m^2. At both cases, bubbles at the vertical inclination are larger in size and greater in number than at the horizontal inclination. This can also be seen in the comparisons between the snapshots of high speed videos at *ae* = 3 g, G = 330 kg/m^2 s and q″ = 690 kW/m^2. The above indicate a greater difficulty for heat transfer in the vertical inclination. Indeed, for the same *ae*, G and q″ values the value of ΔT_{wall} is significantly higher at the vertical inclination which confirms the difficulty. Supplementary Video S7 shows a high speed video recorded at *ae* = 3 g, G = 330 kg/m^2 s, q″ = 690 kW/m^2 and for vertical channel

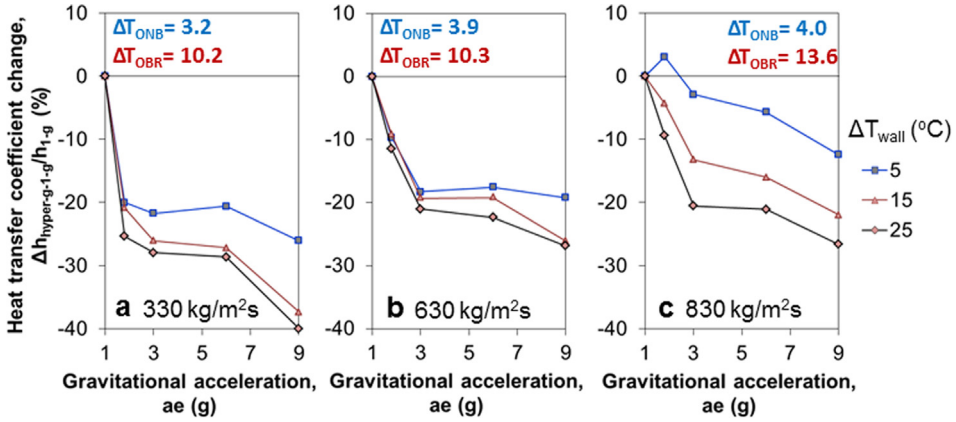

Fig. 12. Percentage change of heat transfer coefficient with gravitational acceleration for vertical channel inclination and water mass flux at (a) 330, (b) 630, (c) 830 kg/m^2 s. *ONB: onset of nucleate boiling, OBR: onset of bubbly regime.*

Table 4
Images for vertical channel inclination at 330 kg/m^2 s.

ae (g)	q'' (kW/m^2)	ΔT_{wall} (°C)	Photograph from the side window
3.0 ***	690	26.8	
9.0	520	11.2	
	600	15.9	
	750	21.6	
	850	23.7	
	900	30.0	

*** *snapshot of high-speed video recording/ Supplementary S6* 1 mm

Video shoots from a small angle above the boiling surface and targets the interior of the boiling surface

inclination. The images are less distorted compared to the video for the horizontal inclination because of the more homogenous water temperature in the motoring area (suppressed thermal boundary layer, no agitation). It is seen that bubbles are dense on the boiling surface, and in many cases bounce repeatedly up and down at the boiling surface, coalescence with neighboring bubbles and re-attach on it. Once in a while a very large bubble appears that scavenges many smaller bubbles along its path. Optical observations are in line with thermal results, according to which vertical inclination promotes bubbles sliding along the boiling surface and enhances their coalescence so a large part of the boiling surface is covered by vapor, whereas in the horizontal inclination bubbles detachment is favored so heat transfer is boosted.

4.3. Effect of channel inclination on boiling curves under Earth-gravity and hyper-gravity

The effect of channel's inclination is not the same at 1-g and hyper-g conditions, since hyper-gravity has different effect in the two inclinations. Comparison of the boiling curves between horizontal and vertical inclination at all experimental conditions is illustrated in Supplementary Fig. S8. At 1 g boiling curves lie almost on top of each other until a certain ΔT_{wall} value, above which the vertical inclination becomes slightly more efficient, only for the low G, 330 kg/m^2 s, because of domination of nucleate boiling, OBR, occurs at a bit lower ΔT_{wall} [9]. At high-g the situation is reversed; although ONB and OBR for the vertical inclination occur at lower q″ and lower ΔT_{wall}, the boiling curves show that the horizontal channel is more efficient. This is in agreement with the discussion in the previous section and can be related to the observed flow patterns for the two inclinations. In the horizontal inclination hyper-gravity acts normal to the heated wall, promotes bubbles detachment, and this is evident from the smaller number of bubbles observed on the boiling surface (i.e. Table 2, 9.0 g). In the vertical inclination hyper-gravity acts parallel to the heated wall, promotes bubbles sliding and bouncing, and this is evident from the larger and more bubbles that appear attached to the boiling surface (i.e. Table 4, 9.0 g).

The percentage variation of h when changing channel's inclination from vertical to horizontal is presented in Fig. 13. Again, results refer to three ΔT_{wall} values for every examined G value. It is quite remarkable that h_{hor} is ~20 to ~40% higher than h_{ver}. These percentage variations are much larger, than those found when changing the channel's geometry [8,9]. It is worth mentioning that

Table 5
Images for vertical channel inclination at 830 kg/m^2 s.

ae (g)	q'' (kW/m^2)	ΔT_{wall} (°C)	Photograph from the side window
1.8	770	5.2	
	850	11.2	
	900	28.1	
3.0	750	17.8	
	900	28.6	
6.0	680	2.2	
	850	24.0	
9.0	770	13.7	
	850	21.1	

1 mm

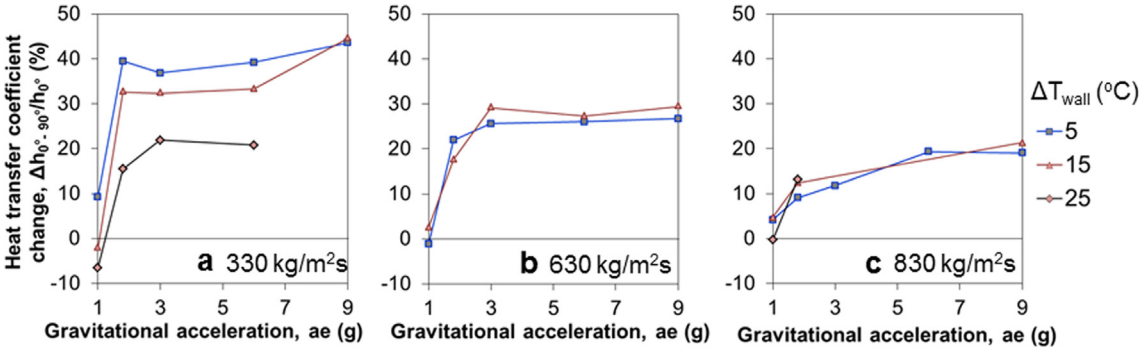

Fig. 13. Percentage change of heat transfer coefficient between the horizontal and the vertical channel inclination for all examined gravitational acceleration levels and water mass flux at (a) 330, (b) 630 and (c) 830 kg/m^2 s.

Xie et al. [17] also reported different effect of hyper-gravity on flow boiling heat transfer in a helical coil at different orientations (axial and radial). According to their results obtained at hyper-gravity conditions, in the radial configuration (similar to the horizontal one of the current work) the heat transfer coefficient increases up to 60%, while in the axial configuration (similar to the vertical one of the current work) h decreases between 40% and 80%. Their complicated helical coil geometry makes it difficult to explain this variant behavior, but it seems that the centripetal acceleration from the coil curvature suppresses hyper-gravity effects. According to the present work, the relative direction of the flow with respect to the inclination of the boiling surface is important, because it dictates whether bubble buoyancy and liquid natural convection play a role or not.

4.4. Comparison of heat transfer coefficient with empirical models

The two-phase heat transfer data of the current research at 1 g and high-g are compared with two existing correlations estimating the flow boiling heat transfer coefficient at Earth's gravity; the one developed by Liu and Winterton [28] in 1991, and a recent one, developed in 2017, by Shah [29]. The range of values of the present experimental parameters (water, G, q″, D_h, *Re*, p_r, *Bo*, ΔT_{sub}, ΔT_{wall}) falls within the range of applicability of these correlations. None of the two models includes a gravity related parameter; nevertheless, it is examined here whether they are still able to describe hyper-gravity results, given their relatively broad uncertainty range. Comparative results between experimental and theoretical h values are presented in Fig. 14. MAPE of each *ae* is listed in Table 6. Regarding Liu-Winterton's correlation, all our experimental data fall within the model's uncertainty range with an average MAPE of 28.7%. Furthermore, it is observed (although hard to discern in the plot), that as *ae* increases, h values systematically shift towards the 0% line, with the 9 g experimental results being really close to the theoretical values. Concerning Shah's correlation, most of our experimental data fall within model's uncertainty range with an average MAPE of 25.0%. In this case the data are more scattered, and moreover there exist extreme outliers from the model's uncer-

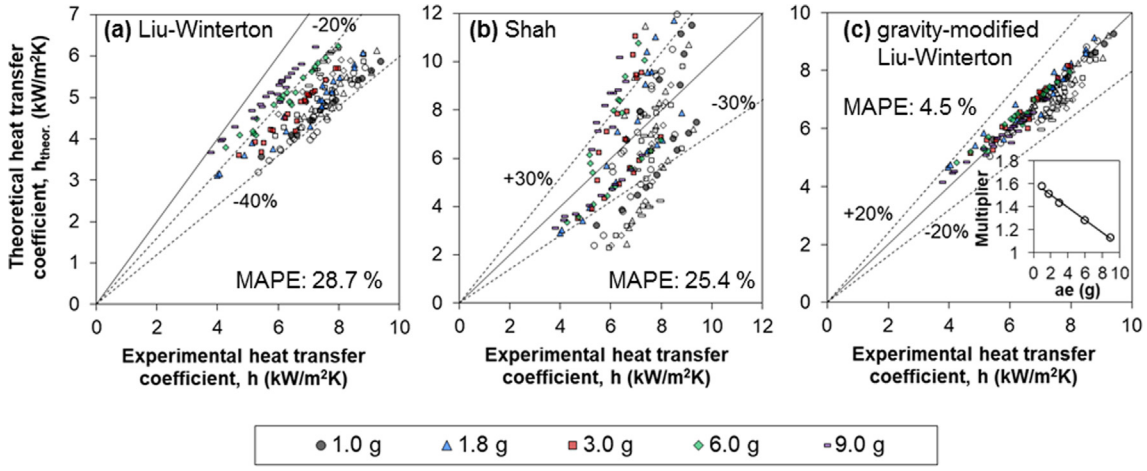

Fig. 14. Comparison between present experimental values of heat transfer coefficient and values estimated from the correlations of (a) Liu and Winterton [27], (b) Shah [28] and (c) gravity-modified Liu and Winterton. *Empty symbols stand for horizontal and filled symbols for vertical inclination. For figure (c) data are jointly for the horizontal and vertical inclinations and exclusively for bubbly flow conditions.*

Table 6
Deviation from the correlations (MAPE).

Correlation	1 g	1.8 g	3 g	6 g	9 g
Horizontal					
Liu-Winterton [24]	38.8	36.1	33.1	27.7	21.4
Shah [25]	22.2	29.8	30.8	28.6	26.1
Vertical					
Liu-Winterton [24]	37.2	31.1	28.5	17.3	9.6
Shah [25]	23.5	22.6	23.8	23.1	26.5

tainty range for high G and q″ values (above +30%) and for low G and q″ values (below −30%).

All in all, Earth-gravity and hyper-gravity results are sufficiently described by the aforementioned equations in view of their broad range of uncertainty. However, it seems that hype-gravity results would be better described by Liu-Winterton's model if a gravity-dependent term is added to eliminate the systematic shift of predicted values when increasing hyper-gravity. By manipulating the predictions by Liu-Winterton model to fit better the present experimental data (ae range: 1.0–9.0 g), a multiplier is found, which is linearly dependent on gravitational acceleration (Fig. 14c).

$$h_{g\text{-modified}} = m \cdot h_{L\text{-}W} \tag{23}$$

$$m = -0.054694 \cdot ae + 1.61135 \tag{24}$$

where $h_{g\text{-modified}}$ is the gravity-modified Liu-Winterton prediction for two phase flow boiling heat transfer coefficient based on the present experimental data, $h_{L\text{-}W}$ is the prediction from Liu-Winterton model for 1-g conditions, m is the gravity dependent multiplier and ae is the gravitational acceleration (g).

This gravity-modified version of Liu-Winterton, valid for gravitational accelerations from 1.0 g to 9.0 g, yields a 4.5% MAPE with all data falling within ±20% of predictions.

5. Conclusions

Flow boiling experiments in a macro-channel (height 3 mm, width 40 mm, length 120 mm) are conducted under Earth-gravity and hyper-gravity in order to explore the role of bubble buoyancy and liquid natural convection in the heat transfer mechanism. Water is used as working fluid at an average ambient temperature 25 °C, (average subcooling at 1.0 g, ΔT_{sub} = 75 °C), at three mass fluxes, 330, 630 and 830 kg/m^2 s and at heat fluxes between 200 and 900 kW/m^2. For the purpose of comparison, two channel inclinations are examined, horizontal, where gravitational acceleration is normal to the heated wall, and vertical, where gravitational acceleration is parallel to the heated wall at a direction opposite to the flow. The conclusions can be summarized as follows:

- The difference between the two-phase (in the presence of vapor bubbles) heat transfer coefficient under hyper-gravity and under Earth-gravity is significant and varies with channel inclination. For the horizontal case, hyper-gravity heat transfer coefficient is ∼10–15% higher than that at Earth-gravity. This is so even for low hyper-gravity levels (*ae* = 1.8 g). For the vertical case, however, hyper-gravity heat transfer coefficient is ∼10–40% lower than that at Earth-gravity.
- In the horizontal inclination, hyper-gravity enhances heat transfer mechanism probably via the following process: high-g intensifies liquid natural convection and promotes bubbles buoyancy (i.e., detachment), which causes agitation of the thermal layer close to the heated wall.
- In the vertical inclination, hyper-gravity deteriorates heat transfer most likely because bubbles buoyancy and liquid natural convection currents are unable to promote bubbles detachment. On the contrary, bubbles are sliding along the boiling surface increasing the chances for coalescence and leading to a temporary coverage of part of the boiling surface by vapor. The situation becomes worse as ΔT_{wall} increases because of the higher bubble population density.

- As gravitational acceleration increases, ΔT_{wall} at which onset of nucleate boiling, ONB, and onset of bubbly regime, OBR, occur remains the same. On the other hand, q'' increases, but only for the horizontal channel, indicating an increased CHF.
- As mass flux increases, forced convection contribution becomes more significant, and therefore suppresses the hyper-gravity effect on bubbles buoyancy and liquid natural convection.
- A gravity-modified Liu-Winterton model is proposed by the introduction of a simple multiplier to predict quite well hyper-gravity flow boiling heat transfer coefficient values. This multiplier decreases linearly with increasing gravitational acceleration.

Conflict of interest

On behalf of all the authors I wish to confirm that there are no known conflicts of interest associated with this publication.

Acknowledgements

This research was supported by the European Space Agency (Co. No. 4000106405/12/NL/PA on highly efficient flow boiling macrostructured/ macroporous channels & MANBO, MAP Project AO-2004-111 Co. No. 4200020289) and by IKY Fellowships of Excellence for Postgraduate Studies in Greece (the SIEMENS Program). The work was performed under the umbrella of COST Action MP1106. We also like to thank Mr. Alan Dowson for his support for this study.

Appendix A. Supplementary data

Supplementary data associated with this article can be found, in the online version, at https://doi.org/10.1016/j.ijheatmasstransfer.2018.12.086.

References

[1] J.F. Tullius, R. Vajtai, Y. Bayazitoglu, A review of cooling in microchannels, Heat Transfer Eng. 32 (2011) 527–541.
[2] A. Sitar, I. Sedmak, I. Golobic, Boiling of water and FC-72 in microchannels enhanced with novel features, Int. J. Heat Mass Transf. 55 (2012) 6446–6457.
[3] D. Deng, W. Wan, H. Shao, Y. Tang, J. Feng, J. Zeng, Effects of operation parameters on flow boiling characteristics of heat sink cooling systems with reentrant porous microchannels, Energy Convers. Manage. 96 (2015) 340–351.
[4] B. Markal, O. Aydin, M. Avci, Effect of aspect ratio on saturated flow boiling in microchannels, Int. J. Heat Mass Transf. 93 (2016) 130–143.
[5] S. Zhang, W. Yuan, Y. Tang, J. Chen, Z. Li, Enhanced flow boiling in an interconnected microchannel net at different inlet subcooling, Appl. Therm. Eng. 104 (2016) 659–667.
[6] S.M. Ghiaasiaan, Two-Phase Flow, Boiling and Condensation in Conventional and Miniature Systems, Cambridge University Press, New York, 2008.
[7] B.G. Suhas, A. Sathyabhama, Bubble dynamics of water-ethanol mixture during subcooled flow boiling in a conventional channel, Appl. Therm. Eng. 113 (2017) 1596–2609.
[8] M.C. Vlachou, J.S. Lioumbas, K. David, D. Chasapis, T.D. Karapantsios, Effect of channel height and mass flux on highly subcooled horizontal flow boiling, Exp. Therm. Fluid Sci. 83 (2017) 157–168.
[9] M.C. Vlachou, T.D. Karapantsios, Effect of channel inclination on heat transfer and bubble dynamics during subcooled flow boiling, Int. J. Therm. Sci. 124 (2018) 484–495.
[10] W.M. Rohsenow, J.P. Hartnett, Y.I. Cho, Handbook of Heat Transfer, McGraw-Hill, USA, 1998.
[11] H. Ohta, Experiments on microgravity boiling heat transfer by using transparent heaters, Nucl. Eng. Des. 175 (1997) 167–180.
[12] S. Luciani, D. Brutin, C. Le Niliot, O. Rahli, L.S. Tadrist, Flow boiling in minichannels under normal, hyper-, and microgravity: Local heat transfer analysis using inverse methods, J. Heat Transf. 130 (2008) 101502.
[13] H. Zhang, I. Mudawar, M.M. Hasan, Application of flow boiling for thermal management of electronics in microgravity and reduced-gravity space systems, IEEE Trans. Compon. Packag. Technol. 32 (2009) 466–477.
[14] C. Baltis, G.P. Celata, M. Cumo, L. Saraceno, G. Zummo, Gravity influence on heat transfer rate in flow boiling, Microgravity Sci. Technol. 24 (2012) 203–213.
[15] C.M. Valencia-Castillo, G.P. Celata, L. Saraceno, G. Zummo, Visual analysis of flow boiling at different gravity levels in 4.0 mm tube, ASME J. Phys. Conf. Ser. 547 (2014) 012029.
[16] C. Konishi, H. Lee, I. Mudawar, M.M. Hasan, H.K. Nahra, N.R. Hall, J.D. Wagner, R.L. May, J.R. Mackey, Flow boiling in microgravity: Part 1 – interfacial behavior and experimental heat transfer results, Int. J. Heat Mass Transf. 81 (2015) 705–720.
[17] L. Xie, Y. Xie, H. Wu, J. Yu, High gravity influence on boiling heat transfer in helical coils, Int. J. Heat Mass Transf. 73 (2014) 706–715.
[18] Y. Xu, X. Fang, G. Li, D. Li, An experimental investigation of flow boiling heat transfer and pressure drop of R134a in a horizontal 2.168mm tube under hypergravity. Part II: Heat transfer coefficient, Int. J. Heat Mass Transf. 80 (2015) 597–604.
[19] X. Fang, G. Li, D. Li, Y. Xu, An experimental study of R134a flow boiling heat transfer in a 4.07mm tube under Earth's gravity and hypergravity, Int. J. Heat Mass Transf. 87 (2015) 399–408.
[20] W.H. Jens, P.A. Lottes, Analysis of Heat Transfer, Burnout, Pressure Drop and Density Data for High Pressure Water, Report 22/ANL-4627, United States Atomic Energy Commission, 1951.
[21] J.R.S. Thorn, W.M. Walker, T.A. Fallon, G.F.S. Reising, Boiling in sub-cooled water during flow up heated tubes or annuli, SAGE J. 180 (1965) 226–246.
[22] S.L. Qi, P. Zhang, R.Z. Wang, L.X. Xu, Flow boiling of liquid nitrogen in micro-tubes: Part II – heat transfer characteristics and critical heat flux, Int. J. Heat Mass Transf. 50 (2007) 5017–5030.
[23] B.R. Munson, D.F. Young, T.H. Okiishi, W.W. Huebsch, Fundamentals of Fluid Mechanics, John Wiley & Sons Inc, United States of America, 2009.
[24] V.D.I. Atlas, VDI Heat Atlas, Springer, Germany, 2010.
[25] V. Gnielinski, New equations for heat and mass transfer in turbulent pipe and channel flow, Int. Chem. Eng. 16 (1976) 359–368.
[26] F.W. Dittus, L.M.K. Boelter, Heat Transfer in Automobile Radiators of the Tubular Type, University of California Press, California, 1930.
[27] R.H.S. Winterton, Heat Transfer, Oxford University Press, Oxford, 1997.
[28] Z. Liu, E.H.S. Winterton, A general correlation for saturated and subcooled flow boiling in tubes and annuli, based on a nucleate pool boiling equation, Int. J. Heat Mass Transf. 32 (1991) 2759–2766.
[29] M.M. Shah, New correlation for heat transfer during subcooled boiling in plain channels and annuli, Int. J. Therm. Sci. 112 (2017) 358–370.
[30] J.S. Lioumbas, J. Krause, T.D. Karapantsios, Hypergravity to explore the role of buoyancy in boiling in porous media, Microgravity Sci. Technol. (2012).
[31] ESA, Experimental Data Set (64th Parabolic Flight Campaign), Bordeaux, 2016.
[32] H. Ohta, Heat transfer mechanisms in microgravity flow boiling, Ann. N. Y. Acad. Sci. 974 (2002) 463–480.
[33] S. Luciani, D. Brutin, C. Le Niliot, L. Tadrist, O. Rahli, Boiling heat transfer in a vertical microchannel: local estimation during flow boiling with a non intrusive method, Multiph. Sci. Tech. 21 (2009) 297–328.